High efficiency second harmonic generation in coupled nano Fabry-Perot thin resonators

Tomasz Matthia, Baptiste Fix, Léna Soun, Christophe Dupuis, Nathalie Bardou, Patrick Bouchon

High efficiency second harmonic generation in coupled nano Fabry-Perot thin resonators

TOMASZ MATTHIA[1], BAPTISTE FIX[1,*], LÉNA SOUN[1,2], CHRISTOPHE DUPUIS[2], NATHALIE BARDOU[2], AND PATRICK BOUCHON[1]

[1] DOTA, ONERA, Université Paris-Saclay, F-91123 Palaiseau, France
[2] Center for Nanosciences and Nanotechnology (C2N) - CNRS, Université Paris-Saclay, 10 Boulevard Thomas Gobert, 91120 Palaiseau, France
[*] Corresponding author: baptiste.fix@onera.fr

Compiled July 13, 2022

In this paper we experimentally demonstrate SHG enhancement in thin 1D periodic plasmonic nanostructures on GaAs in the infrared spectral range. Due to the properly designed coupling of horizontal Fabry-Perot nanoresonators that occur inside these structures, the obtained conversion efficiencies go up to the 10^{-7} W^{-1} range. Moreover, we demonstrate that the engineering of the plasmonic nanoantennas dimensions on the same GaAs layer can lead to SHG enhancement for pump wavelength ranging from 2.8 µm to 3.3 µm.

Thin nanostructured metasurfaces have the property of trapping and locally concentrating the incoming light in a subwavelength volume [1]. This ability to highly enhance local optical fields is particularly interesting for exciting naturally weak nonlinear optical effects. Moreover, these structures tackle some of the most challenging issues of conventional devices based on macroscopic bulk nonlinear media such as the need of phase-matching, the limited operational wavelength ranges and the size-related challenges [2–7]. Second order generation (SHG) has been demonstrated with all-dielectric devices based on nonlinear materials nanostructured so as to form nanocylinders [8–11], gratings [12–14] or waveguides [15]. These all-dielectric SHG metasurfaces have demonstrated conversion efficiencies going as high as $\Pi_{SHG} = 10^{-5}$ W^{-1} for a conversion from the telecom to visible wavelength [16]. Such efficiencies have not yet been reached in the mid-infrared. Metallic metamaterials have also been investigated for SHG and among those, two categories can be distinguished. First, those that exploit the centrosymmetric breakdown at the metal surface, where the localized surface plasmon resonance induces strong local field enhancement [17–23]. However, the efficiency of those devices is limited by the ohmic losses occurring in the metal [3]. Second, the use of plasmonic nanostructures that trap and locally concentrate the optical fields inside the volume of a highly nonlinear layer [24–27]. This associates the advantages of both worlds, the intrinsic nonlinearities of high $\chi^{(2)}$ bulk media with the high field enhancement provided by plasmonic devices. Multiple quantum wells has been integrated to such resonators and demonstrated to reach efficiencies as high as 10^{-2} W^{-1} [28–31]. However, these devices are inherently spectrally limited to the quantum well intersubband transitions. On the other hand, even if it leads to weaker efficiencies, exploiting the intrinsic nonlinearities of a high $\chi^{(2)}$ bulk media included in a plasmonic resonator enables the conversion for any spectral range. For instance, metal-insulator-metal (MIM) nanoresonators, supporting Fabry-Perot resonances and including a gallium arsenide (GaAs) layer, have been demonstrated to reach efficiencies as high as 10^{-9} W^{-1} in the mid-infrared [26].

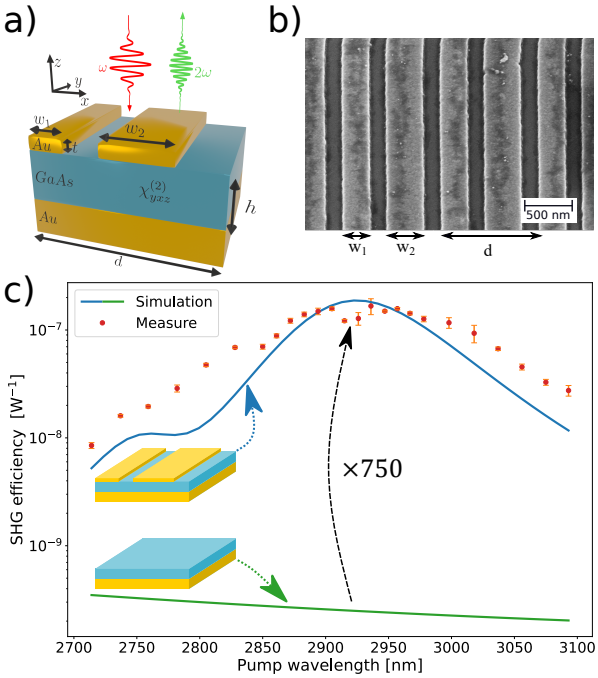

Fig. 1. a) Schematic representation of the resonator. b) A scanning microscope image of the sample. c) The measured and simulated SHG efficiency spectra of the coupled resonator nanostructure. The resulting efficiency is 750 times higher compared to a non-engineered equivalent GaAs layer reference.

In this Letter, we investigate coupled GaAs plasmonic

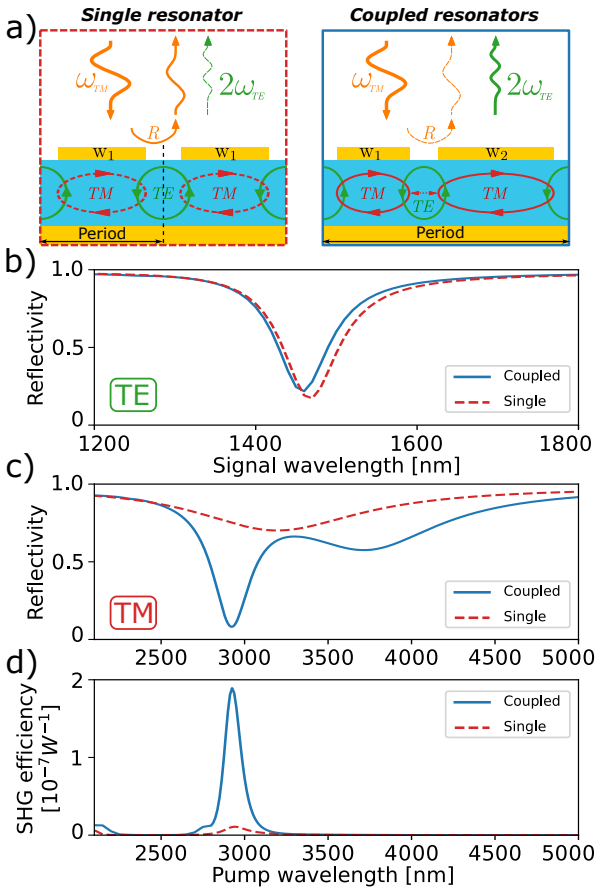

Fig. 2. a) Schematic explanation of the single and coupled FP resonators behavior for the SHG. b) Simulated linear reflectivity of the single resonator (red dashed) and coupled resonators (plain blue) structure at TE-polarized signal frequency. c) Simulated linear reflectivity of the single resonator (red dashed) and coupled resonators (plain blue) structure at TM-polarized pump frequency. d) Simulated nonlinear SHG efficiency of the single resonator (red dashed) and coupled resonators (plain blue) structure at pump frequency.

nanocavities and experimentally demonstrate a high SHG efficiency in the range of 10^{-7} W^{-1} for a mid-wave infrared pump. We show that coupled nano Fabry-Perot resonances enable a 20-fold increase in SHG efficiency with regards to their classical single cavity counterpart. Finally, we experimentally demonstrate SHG on three arrays fabricated on the same GaAs layer for pump wavelength ranging from 2.8 µm to 3.3 µm which evidences the tunability of the resonators.

The studied periodic nanostructure (see Fig. 1 a)), is composed of three layers: a back gold mirror, a thin ($h = 142$ nm) layer of (100)-oriented GaAs crystal whose lattice vectors are aligned along (xyz) and a thin ($t = 60$ nm) top periodic nanostructured gold mirror composed of two equally spaced ribbons. It has been simulated with the B-spline modal method (BMM) [32, 33] as infinite along y and infinitely periodic along x. The model of gold used here is a Drude model in agreement with experimental data in the infrared range: $\epsilon_{Au}(\lambda) = 1 - 1/(\lambda_P/\lambda(\lambda_P/\lambda + i\gamma))$ with $\lambda_P = 159$ nm and $\gamma = 0.0075$ [34]. The nanostructure, defined by a period $d = 1010$ nm, and two ribbons of respective widths $w_1 = 260$ nm and

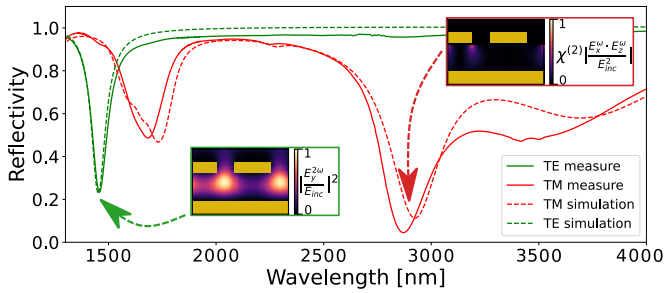

Fig. 3. Simulated and measured linear reflectivities of the structure. In inset the simulated normalized field component amplitudes in the structure at pump ($\lambda_{\text{pump}} = 2.93$ µm) and signal ($\lambda_{\text{signal}} = 1.46$ µm) resonances.

$w_2 = 380$ nm, has been optimized to display a resonance at both the pump wavelength $\lambda_{\text{pump}} = 2.93$ µm and the signal wavelength $\lambda_{\text{signal}} = 1.46$ µm. Indeed, as it has been previously described [25, 35], the two resonances are used to enhance the nonlinear process of light generation.

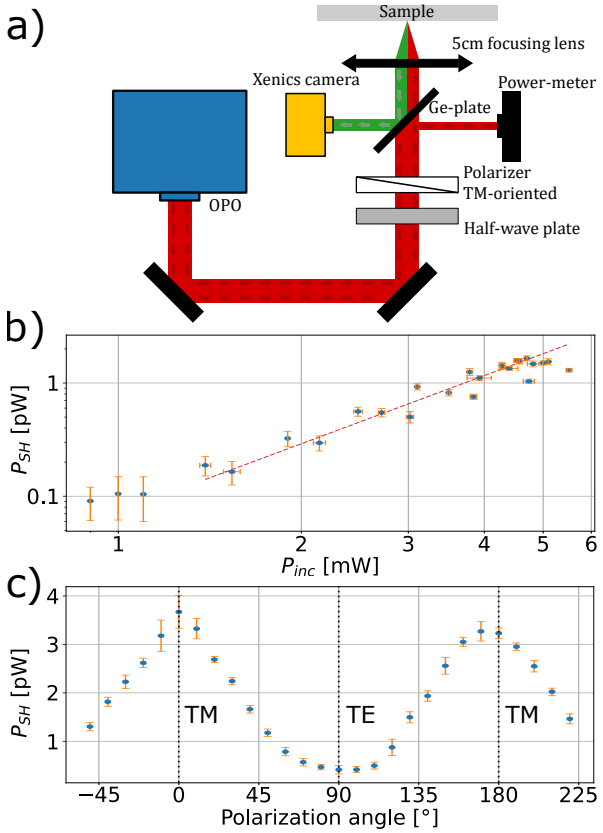

Fig. 4. a) Schematic of the non linear characterisation set-up b) The measured second-harmonic signal power as a function of the incident pump power. The red line is a least-square regression corresponding to the following mathematical expression: $\log(P_{SH}) = 2 \cdot \log(P_{inc}) - 1.138$. c) The second-harmonic signal power as a function of the incident pump polarization angle.

Moreover, the GaAs is a zync-blende crystal whose only non-zero components of the second-order nonlinear susceptibility

tensor are [36]:

$$\chi_{ijk} = \begin{cases} 150 \frac{pm}{V} \Leftrightarrow i \neq j \neq k \\ 0, \quad \text{otherwise} \end{cases} \quad \textbf{(1)}$$

Where $i, j, k \in \{x, y, z\}$. Thus, the whole SHG process can be mathematically summarized in the form of the following expression:

$$E_i{}^{2\omega} \propto \sum_{jk} \chi_{ijk}{}^{(2)} \cdot E_j{}^{\omega} \cdot E_k{}^{\omega} \quad \textbf{(2)}$$

Where $E_i{}^{\omega}$ is the i-axis directed electric field at the frequency of ω. With the 1D periodic structure described, the only solution available consists in a TM-polarized (along the x-axis) pump wave and TE-polarized signal wave (along the y-axis).

The structure simulated and measured SHG efficiencies are presented in Fig. 1 c). It has been calculated using the common linearized formula :

$$\Pi_{SHG} = \frac{P_{SH}}{P_{inc}{}^2} \left[W^{-1}\right] \quad \textbf{(3)}$$

Where P_{SH} and P_{inc} are respectively the power of the generated second-harmonic beam and the power of the incident pump beam. The peak efficiency of 1.69×10^{-7} W^{-1} is achieved at 2.93 µm which represents a 750-fold increase with regard to an equivalent unstructured device.

The optimization of the SHG requires to efficiently trap the pump light inside the GaAs layer and to extract the signal light. This means that, at the two resonances, the cavity modes must be critically coupled to the incident light : the reflectivity of the structure has to be minimized [26]. Among the different available nanostructures, the combination of TE orientated vertical and TM orientated horizontal Fabry-Perot (FP) resonators are well suited for SHG due to their stability with regards to the angle of incidence and the localisation of the concentrated fields. However, the two resonators critical coupling are not compatible due to the high impact of the GaAs layer thickness on both these resonators. To achieve the critical coupling of both resonances, a newly described type of horizontal FP resonance has been used [37]. Indeed, this "coupled Fabry-perot" resonance is based on two spectrally closed under-coupled FP (*i.e.*, with high reflectivity at resonance) that couple with one another. While most properties of the horizontal FP are retained, the resulting resonance is mostly independant from the GaAs layer thickness. The critical coupling is achieved through the optimization of the width difference between the two ribbons.

The impact of using either horizontal FP or coupled FP on the SHG efficiency is illustrated in Fig. 2. On the one hand, the vertical Fabry-Perot resonance is only slightly influenced by the widening of the second ribbons from $w_1 = 260$ nm to $w_2 = 380$ nm. On the other hand, the structure reflectivity at the pump wavelength is drastically reduced from a 75% to 5% leading to a 20-fold increase of the simulated SHG efficiency. Those theoretical results are also congruent with the comparison of the experimental results obtained here (peak of 1.69×10^{-7} W^{-1}) and in analogue single Fabry-Perot resonator structures (peak of 0.8×10^{-8} W^{-1}) [26].

The sample was fabricated first by epitaxial growing of a (100)-oriented layer of GaAs, and depositing it on a Ti/Au/Ti/Al stack in order to create the golden mirror. After mechanical polishing and chemical etching, the golden nanoantennas were deposited by an electron beam lithography process. The structure includes respectively: a golden substrate, a 2 nm thick titanium layer, a 142 nm thick GaAs nonlinear layer, a layer of Al_2O_3 of 10 nm, a grating of 4 nm titanium adhesion layer placed under 60 nm golden nanoantennas. The sample contains several 300 µm width square shaped structures.

The TE and TM linear reflectivity spectrum (see Fig. 3) of the structure have been measured using a FTIR microscope (Bruker Hyperion 2000) and a Cassegrain objective (NA=0.4) with high accordance to the simulated values. The simulated normalized electric field components taking part in the SHG process at both $\lambda_{pump} = 2.92$ µm (TM) and $\lambda_{signal} = 1.46$ µm (TE) wavelength are shown in Fig. 3.

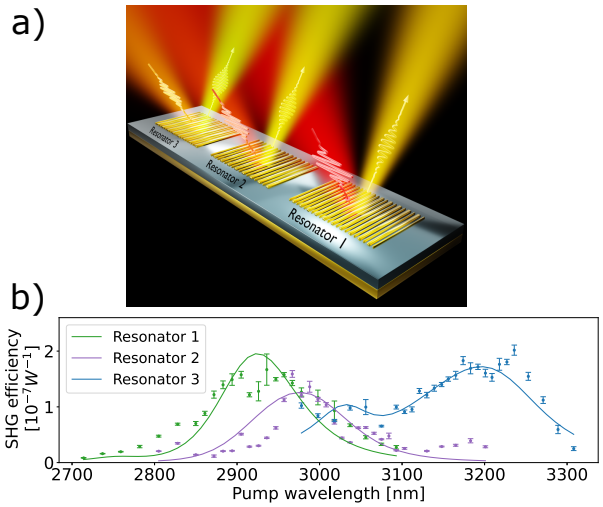

Fig. 5. a) An illustration of the concept of a broad-band SHG nanodevice. b) Measured and simulated SHG conversion efficiency spectra obtained for $w_1 = 295\ nm, w_2 = 350\ nm$, $d = 1215\ nm$ (blue line), $w_1 = 280\ nm, w_2 = 365\ nm$, $d = 1015\ nm$ (purple line) and the structure from Fig. 1 c) (green line). All three resonators have been designed using the same thicknesses of the golden nanoantennas $t = 60\ nm$ and the GaAs nonlinear layer $h = 142\ nm$.

The non linear characterisation set-up is illustrated in Fig. 4 a). The incident pump light is provided by the idler output of an APE nanoLevante optical parametric oscillator (OPO). The laser beam repetition rate is equal to 20 kHz and the peak power density is equal to 0.58 $\frac{\text{MW}}{\text{cm}^2}$. The beam direction of polarization is adjusted to be TM, with respect to the sample geometry, by a half-wave plate.

An additional polarizer can be introduced before the half-wave plate to regulate the incident optical power. The beam is focalized on the sample by a 5 cm CaF_2 focal lens, resulting in a focal spot of 37 µm diameter and an aperture angle of 9 degrees. The generated second-harmonic beam is collimated by the same lens and is reflected by dichroic plate (Ge) towards a Xenics Xeva-1.7-320 SWIR camera. The incident pump light is monitored by measuring the 10% pump power reflected by the Ge plate. Due to its thickness, the germanium plate also introduces a walk-off of the pump beam with regards to the center of the focusing lens, resulting in an mean incident angle of about 4.5°. The evolution of the second harmonic beam generation with the incident pump power and the direction of polarization is presented in Fig. 4. The SH generation power follow the expected quadratic dependency with the incident pump. Moreover, the SHG process depends on the TM polarisation of the pump which is confirmed by the relation of the SH power with the direction of polarisation.

Noteworthily, a wide variety of resonance wavelength can be achieved for both cavities while the nonlinear material thickness is maintained constant. Indeed, as illustrated in Fig. 5, the nonlinear generation can be spectrally shifted by varying the period of the structure as well as the width of each of the plasmonic nanorods. The first resonator (green line) is the one that has been presented in Fig. 1. The two additional SHG structures have been obtained for $w_1 = 280$ nm, $w_2 = 365$ nm, $d = 1015$ nm (purple line) and $w_1 = 295$ nm, $w_2 = 350$ nm, $d = 1215$ nm (blue line) to have a peak generation for a pump at 2.8 μm and 3.24 μm respectively. The two structures have been characterised through the same set-up.

In conclusion, we have theoretically and experimentally studied the properties of multiresonant MIM structures optimized for the SHG. Due to an increased pump light absorption, the coupling of two horizontal Fabry-Perot nano-resonators provides a 20-fold increase in the obtained efficiencies. This increase enables us to attain the 10^{-7} W^{-1} efficiency range in bulk GaAs for wavelength ranging from $\lambda = 2.8$ μm to $\lambda = 3.3$ μm. The measured efficiencies are in good agreement with the theoretical predictions. This advancement paves the way to more efficient nonlinear plasmonic nanodevices. Moreover, those devices can be spectrally adjusted without modifying the substrate and the GaAs layer (see Fig. 5 and the supplement). This gives the possibility, either of creating discrete arrays of different resonators, or combining them into a single wide-spectrum converter. Different approaches may be studied in order to further increase the SHG efficiency. First, the use of a different set of resonances could improve the spatial mode overlap. Finally, the interaction between the electric fields and the nonlinear layer could be enhanced by better fitting the components of the nonlinear susceptibility tensor or by using multiple quantum wells.

Funding. This work is supported by a DGA - Agence Innovation Défense scholarship.

Disclosures. The authors declare no conflicts of interest.

Data Availability Statement. All numerical and experimental data are available on request from the authors.

Supplemental document. See Supplement 1 for supporting content.

REFERENCES

1. P. Bouchon, F. Pardo, B. Portier, L. Ferlazzo, P. Ghenuche, G. Dagher, C. Dupuis, N. Bardou, R. Haïdar, and J.-L. Pelouard, Appl. Phys. Lett. **98**, 191109 (2011).
2. J. A. Schuller, E. S. Barnard, W. Cai, Y. C. Jun, J. S. White, and M. L. Brongersma, Nat. Mater. **9**, 193 (2010).
3. M. Kauranen and A. V. Zayats, Nat. Photonics **6**, 737 (2012).
4. S. Keren-Zur, L. Michaeli, H. Suchowski, and T. Ellenbogen, Adv. Opt. Photonics **10**, 309 (2018).
5. N. C. Panoiu, W. E. I. Sha, D. Y. Lei, and G.-C. Li, J. Opt. **20**, 083001 (2018).
6. A. Krasnok, M. Tymchenko, and A. Alù, Mater. Today **21**, 8 (2018).
7. A. P. Anthur, H. Zhang, R. Paniagua-Dominguez, D. A. Kalashnikov, S. T. Ha, T. W. W. Maß, A. I. Kuznetsov, and L. Krivitsky, Nano Lett. **20**, 8745 (2020).
8. S. Liu, M. B. Sinclair, S. Saravi, G. A. Keeler, Y. Yang, J. Reno, G. M. Peake, F. Setzpfandt, I. Staude, T. Pertsch, and I. Brener, Nano Lett. **16**, 5426 (2016).
9. V. F. Gili, L. Carletti, A. Locatelli, D. Rocco, M. Finazzi, L. Ghirardini, I. Favero, C. Gomez, A. Lemaître, M. Celebrano, C. D. Angelis, and G. Leo, Opt. Express **24**, 15965 (2016).
10. D. Rocco, V. F. Gili, L. Ghirardini, L. Carletti, I. Favero, A. Locatelli, G. Marino, D. N. Neshev, M. Celebrano, M. Finazzi, G. Leo, and C. D. Angelis, Photonics Res. **6**, B6 (2018).
11. R. Sarma, J. Xu, D. de Ceglia, L. Carletti, S. Campione, J. Klem, M. B. Sinclair, M. A. Belkin, and I. Brener, Nano Lett. **22**, 896 (2022).
12. D. d. Ceglia, G. D'Aguanno, N. Mattiucci, M. A. Vincenti, and M. Scalora, Opt. Lett. **36**, 704 (2011).
13. U. A. Leon, D. Rocco, L. Carletti, M. Peccianti, S. Maci, G. Della Valle, and C. De Angelis, Sci. Reports **12**, 4590 (2022).
14. P. P. Vabishchevich, S. Liu, M. B. Sinclair, G. A. Keeler, G. M. Peake, and I. Brener, ACS Photonics **5**, 1685 (2018).
15. M. Gromovyi, J. Brault, A. Courville, S. Rennesson, F. Semond, G. Feuillet, P. Baldi, P. Boucaud, J.-Y. Duboz, and M. P. D. Micheli, Opt. Express **25**, 23035 (2017).
16. G. Marino, D. Rocco, C. Gigli, G. Beaudoin, K. Pantzas, S. Suffit, P. Filloux, I. Sagnes, G. Leo, and C. D. Angelis, Nanophotonics **10**, 1837 (2021).
17. E. Kim, F. Wang, W. Wu, Z. Yu, and Y. R. Shen, "Nonlinear optical spectroscopy of photonic metamaterials," in *2008 Conference on Lasers and Electro-Optics and 2008 Conference on Quantum Electronics and Laser Science,* (2008), pp. 1–2.
18. V. K. Valev, N. Smisdom, A. V. Silhanek, B. De Clercq, W. Gillijns, M. Ameloot, V. V. Moshchalkov, and T. Verbiest, Nano Lett. **9**, 3945 (2009).
19. H. Husu, R. Siikanen, J. Mäkitalo, J. Lehtolahti, J. Laukkanen, M. Kuittinen, and M. Kauranen, Nano Lett. **12**, 673 (2012).
20. M. Celebrano, X. Wu, M. Baselli, S. Großmann, P. Biagioni, A. Locatelli, C. De Angelis, G. Cerullo, R. Osellame, B. Hecht, L. Duò, F. Ciccacci, and M. Finazzi, Nat. Nanotechnol. **10**, 412 (2015).
21. N. Segal, S. Keren-Zur, N. Hendler, and T. Ellenbogen, Nat. Photonics **9**, 180 (2015).
22. P.-Y. Chen, C. Argyropoulos, G. D'Aguanno, and A. Alù, ACS Photonics **2**, 1000 (2015).
23. L. Chu, Z. Li, H. Zhu, F. Ren, and F. Chen, Appl. Phys. Lett. **120**, 073104 (2022).
24. P.-Y. Chen, C. Argyropoulos, and A. Alù, Nanophotonics **1**, 221 (2012).
25. L. Soun, S. Héron, H. E. Ouazzani, B. Fix, R. Haïdar, R. Haïdar, and P. Bouchon, Opt. Express **28**, 27210 (2020).
26. L. Soun, B. Fix, H. E. Ouazzani, S. Héron, N. Bardou, C. Dupuis, S. Derelle, J. Jaeck, R. Haïdar, R. Haïdar, and P. Bouchon, Opt. Lett. **46**, 1466 (2021).
27. N. Nookala, J. Xu, O. Wolf, S. March, R. Sarma, S. Bank, J. Klem, I. Brener, and M. Belkin, Appl. Phys. B **124**, 132 (2018).
28. F. Capasso, C. Sirtori, and A. Cho, IEEE J. Quantum Electron. **30**, 1313 (1994).
29. O. Wolf, S. Campione, A. Benz, A. P. Ravikumar, S. Liu, T. S. Luk, E. A. Kadlec, E. A. Shaner, J. F. Klem, M. B. Sinclair, and I. Brener, Nat. Commun. **6**, 7667 (2015).
30. J. Lee, M. Tymchenko, C. Argyropoulos, P.-Y. Chen, F. Lu, F. Demmerle, G. Boehm, M.-C. Amann, A. Alù, and M. A. Belkin, Nature **511**, 65 (2014).
31. S. Campione, A. Benz, M. B. Sinclair, F. Capolino, and I. Brener, Appl. Phys. Lett. **104**, 131104 (2014).
32. P. Bouchon, F. Pardo, R. Haïdar, and J.-L. Pelouard, J. Opt. Soc. Am. A **27**, 696 (2010).
33. S. Héron, F. Pardo, P. Bouchon, J.-L. Pelouard, and R. Haïdar, J. Opt. Soc. Am. B **32**, 275 (2015).
34. E. D. Palik, *Handbook of Optical Constants of Solids*, vol. 3 (Academic Press, 1998).
35. Z. Lin, X. Liang, M. Lončar, S. G. Johnson, and A. W. Rodriguez, Optica **3**, 233 (2016).
36. T. Skauli, K. L. Vodopyanov, T. J. Pinguet, A. Schober, O. Levi, L. A. Eyres, M. M. Fejer, J. S. Harris, B. Gerard, L. Becouarn, E. Lallier, and G. Arisholm, Opt. Lett. **27**, 628 (2002).
37. B. Fix, J. Jaeck, P. Bouchon, N. Bardou, B. Vest, and R. Haidar, arXiv preprint arXiv:2011.05242 (2020).

FULL REFERENCES

1. P. Bouchon, F. Pardo, B. Portier, L. Ferlazzo, P. Ghenuche, G. Dagher, C. Dupuis, N. Bardou, R. Haïdar, and J.-L. Pelouard, "Total funneling of light in high aspect ratio plasmonic nanoresonators," Appl. Phys. Lett. **98**, 191109 (2011).
2. J. A. Schuller, E. S. Barnard, W. Cai, Y. C. Jun, J. S. White, and M. L. Brongersma, "Plasmonics for extreme light concentration and manipulation," Nat. Mater. **9**, 193–204 (2010).
3. M. Kauranen and A. V. Zayats, "Nonlinear plasmonics," Nat. Photonics **6**, 737–748 (2012).
4. S. Keren-Zur, L. Michaeli, H. Suchowski, and T. Ellenbogen, "Shaping light with nonlinear metasurfaces," Adv. Opt. Photonics **10**, 309–353 (2018).
5. N. C. Panoiu, W. E. I. Sha, D. Y. Lei, and G.-C. Li, "Nonlinear optics in plasmonic nanostructures," J. Opt. **20**, 083001 (2018).
6. A. Krasnok, M. Tymchenko, and A. Alù, "Nonlinear metasurfaces: a paradigm shift in nonlinear optics," Mater. Today **21**, 8–21 (2018).
7. A. P. Anthur, H. Zhang, R. Paniagua-Dominguez, D. A. Kalashnikov, S. T. Ha, T. W. W. Maß, A. I. Kuznetsov, and L. Krivitsky, "Continuous Wave Second Harmonic Generation Enabled by Quasi-Bound-States in the Continuum on Gallium Phosphide Metasurfaces," Nano Lett. **20**, 8745–8751 (2020).
8. S. Liu, M. B. Sinclair, S. Saravi, G. A. Keeler, Y. Yang, J. Reno, G. M. Peake, F. Setzpfandt, I. Staude, T. Pertsch, and I. Brener, "Resonantly Enhanced Second-Harmonic Generation Using III–V Semiconductor All-Dielectric Metasurfaces," Nano Lett. **16**, 5426–5432 (2016).
9. V. F. Gili, L. Carletti, A. Locatelli, D. Rocco, M. Finazzi, L. Ghirardini, I. Favero, C. Gomez, A. Lemaître, M. Celebrano, C. D. Angelis, and G. Leo, "Monolithic AlGaAs second-harmonic nanoantennas," Opt. Express **24**, 15965–15971 (2016).
10. D. Rocco, V. F. Gili, L. Ghirardini, L. Carletti, I. Favero, A. Locatelli, G. Marino, D. N. Neshev, M. Celebrano, M. Finazzi, G. Leo, and C. D. Angelis, "Tuning the second-harmonic generation in AlGaAs nanodimers via non-radiative state optimization [Invited]," Photonics Res. **6**, B6–B12 (2018).
11. R. Sarma, J. Xu, D. de Ceglia, L. Carletti, S. Campione, J. Klem, M. B. Sinclair, M. A. Belkin, and I. Brener, "An All-Dielectric Polaritonic Metasurface with a Giant Nonlinear Optical Response," Nano Lett. **22**, 896–903 (2022).
12. D. d. Ceglia, G. D'Aguanno, N. Mattiucci, M. A. Vincenti, and M. Scalora, "Enhanced second-harmonic generation from resonant GaAs gratings," Opt. Lett. **36**, 704–706 (2011).
13. U. A. Leon, D. Rocco, L. Carletti, M. Peccianti, S. Maci, G. Della Valle, and C. De Angelis, "THz-photonics transceivers by all-dielectric phonon-polariton nonlinear nanoantennas," Sci. Reports **12**, 4590 (2022).
14. P. P. Vabishchevich, S. Liu, M. B. Sinclair, G. A. Keeler, G. M. Peake, and I. Brener, "Enhanced Second-Harmonic Generation Using Broken Symmetry III–V Semiconductor Fano Metasurfaces," ACS Photonics **5**, 1685–1690 (2018).
15. M. Gromovyi, J. Brault, A. Courville, S. Rennesson, F. Semond, G. Feuillet, P. Baldi, P. Boucaud, J.-Y. Duboz, and M. P. D. Micheli, "Efficient second harmonic generation in low-loss planar GaN waveguides," Opt. Express **25**, 23035–23044 (2017).
16. G. Marino, D. Rocco, C. Gigli, G. Beaudoin, K. Pantzas, S. Suffit, P. Filloux, I. Sagnes, G. Leo, and C. D. Angelis, "Harmonic generation with multi-layer dielectric metasurfaces," Nanophotonics **10**, 1837–1843 (2021).
17. E. Kim, F. Wang, W. Wu, Z. Yu, and Y. R. Shen, "Nonlinear optical spectroscopy of photonic metamaterials," in *2008 Conference on Lasers and Electro-Optics and 2008 Conference on Quantum Electronics and Laser Science,* (2008), pp. 1–2.
18. V. K. Valev, N. Smisdom, A. V. Silhanek, B. De Clercq, W. Gillijns, M. Ameloot, V. V. Moshchalkov, and T. Verbiest, "Plasmonic ratchet wheels: switching circular dichroism by arranging chiral nanostructures," Nano Lett. **9**, 3945–3948 (2009).
19. H. Husu, R. Siikanen, J. Mäkitalo, J. Lehtolahti, J. Laukkanen, M. Kuittinen, and M. Kauranen, "Metamaterials with Tailored Nonlinear Optical Response," Nano Lett. **12**, 673–677 (2012).
20. M. Celebrano, X. Wu, M. Baselli, S. Großmann, P. Biagioni, A. Locatelli, C. De Angelis, G. Cerullo, R. Osellame, B. Hecht, L. Duò, F. Ciccacci, and M. Finazzi, "Mode matching in multiresonant plasmonic nanoantennas for enhanced second harmonic generation," Nat. Nanotechnol. **10**, 412–417 (2015).
21. N. Segal, S. Keren-Zur, N. Hendler, and T. Ellenbogen, "Controlling light with metamaterial-based nonlinear photonic crystals," Nat. Photonics **9**, 180–184 (2015).
22. P.-Y. Chen, C. Argyropoulos, G. D'Aguanno, and A. Alù, "Enhanced Second-Harmonic Generation by Metasurface Nanomixer and Nanocavity," ACS Photonics **2**, 1000–1006 (2015).
23. L. Chu, Z. Li, H. Zhu, F. Ren, and F. Chen, "Second-harmonic generation of embedded plasmonic nanoparticle arrays via interparticle coupling," Appl. Phys. Lett. **120**, 073104 (2022).
24. P.-Y. Chen, C. Argyropoulos, and A. Alù, "Enhanced nonlinearities using plasmonic nanoantennas," Nanophotonics **1**, 221–233 (2012).
25. L. Soun, S. Héron, H. E. Ouazzani, B. Fix, R. Haïdar, R. Haïdar, and P. Bouchon, "4000-enhancement of difference frequency generation in a mode-matching metamaterial," Opt. Express **28**, 27210–27222 (2020).
26. L. Soun, B. Fix, H. E. Ouazzani, S. Héron, N. Bardou, C. Dupuis, S. Derelle, J. Jaeck, R. Haïdar, R. Haïdar, and P. Bouchon, "Experimental demonstration of second-harmonic generation in high x^2 metasurfaces," Opt. Lett. **46**, 1466–1469 (2021).
27. N. Nookala, J. Xu, O. Wolf, S. March, R. Sarma, S. Bank, J. Klem, I. Brener, and M. Belkin, "Mid-infrared second-harmonic generation in ultra-thin plasmonic metasurfaces without a full-metal backplane," Appl. Phys. B **124**, 132 (2018).
28. F. Capasso, C. Sirtori, and A. Cho, "Coupled quantum well semiconductors with giant electric field tunable nonlinear optical properties in the infrared," IEEE J. Quantum Electron. **30**, 1313–1326 (1994).
29. O. Wolf, S. Campione, A. Benz, A. P. Ravikumar, S. Liu, T. S. Luk, E. A. Kadlec, E. A. Shaner, J. F. Klem, M. B. Sinclair, and I. Brener, "Phased-array sources based on nonlinear metamaterial nanocavities," Nat. Commun. **6**, 7667 (2015).
30. J. Lee, M. Tymchenko, C. Argyropoulos, P.-Y. Chen, F. Lu, F. Demmerle, G. Boehm, M.-C. Amann, A. Alù, and M. A. Belkin, "Giant nonlinear response from plasmonic metasurfaces coupled to intersubband transitions," Nature **511**, 65–69 (2014).
31. S. Campione, A. Benz, M. B. Sinclair, F. Capolino, and I. Brener, "Second harmonic generation from metamaterials strongly coupled to intersubband transitions in quantum wells," Appl. Phys. Lett. **104**, 131104 (2014).
32. P. Bouchon, F. Pardo, R. Haïdar, and J.-L. Pelouard, "Fast modal method for subwavelength gratings based on B-spline formulation," J. Opt. Soc. Am. A **27**, 696 (2010).
33. S. Héron, F. Pardo, P. Bouchon, J.-L. Pelouard, and R. Haïdar, "Modal method for second harmonic generation in nanostructures," J. Opt. Soc. Am. B **32**, 275 (2015).
34. E. D. Palik, *Handbook of Optical Constants of Solids*, vol. 3 (Academic Press, 1998).
35. Z. Lin, X. Liang, M. Lončar, S. G. Johnson, and A. W. Rodriguez, "Cavity-enhanced second-harmonic generation via nonlinear-overlap optimization," Optica **3**, 233–238 (2016).
36. T. Skauli, K. L. Vodopyanov, T. J. Pinguet, A. Schober, O. Levi, L. A. Eyres, M. M. Fejer, J. S. Harris, B. Gerard, L. Becouarn, E. Lallier, and G. Arisholm, "Measurement of the nonlinear coefficient of orientation-patterned GaAs and demonstration of highly efficient second-harmonic generation," Opt. Lett. **27**, 628–630 (2002).
37. B. Fix, J. Jaeck, P. Bouchon, N. Bardou, B. Vest, and R. Haidar, "Dark-modes excitation in coupled nano fabry-perot structure induced by symmetry breaking," arXiv preprint arXiv:2011.05242 (2020).